



# Hydrostatic Tube Cyclic Extrusion Compression as a Novel Severe Plastic Deformation Method for Fabricating Long Nanostructured Tubes

M. Eftekhari<sup>1</sup> · G. Faraji<sup>1</sup> · M. Bahrami<sup>1</sup> · M. Baniassadi<sup>1</sup>

Received: 4 March 2021 / Accepted: 25 April 2021 / Published online: 8 September 2021  
© The Korean Institute of Metals and Materials 2021

## Abstract

In this study, hydrostatic cyclic extrusion compression (HTCEC) is introduced as a novel severe plastic deformation technique for producing the relatively long and large ultrafine grained (UFG) and nano-grained tubes. In HTCEC technique, the utilization of pressurized hydraulic fluid between the piece and the die leads to the reduction of the friction force and the required processing load. All of these conditions facilitate the processing of the long and large tubes. Also, during HTCEC process, a movable mandrel is placed inside the hollow tube, which plays a main role in the reduction of the required hydrostatic pressure. To investigate the efficiencies of HTCEC process, aluminum 5052 alloy tubes were processed by HTCEC up to two passes. Then, the mechanical properties and microstructure evolution were examined. After the first pass of HTCEC, tangled and diffused arrangements of dislocations were formed. Then, the second pass of HTCEC resulted in a more refined and more homogeneous UFG microstructure with an average subgrain size of 636 nm, while the average grain size of the initial sample was ~360  $\mu\text{m}$ . Tensile tests and hardness measurements revealed that two passes of HTCEC led to an increase in the yield strength from 98 MPa to 254 MPa (~2.6 times higher), the ultimate strength from 178 MPa to 306 MPa (~1.72 times higher) and the microhardness from ~56 to ~120 Hv (~2.14 times higher). Simultaneously, a decrease in the elongation to failure from 31.6 to 15.4% was observed, which is a small amount compared to the results of other studies. Also, in comparison to one-pass, a more homogeneous microhardness distribution through the thickness was detected in the two-pass processed tube. Fractography evaluations by SEM indicated that predominantly ductile fracture occurred in all samples. Furthermore, the equivalent strain and the pressing load of HTCEC process was evaluated by FEM simulation. It seems that HTCEC process, by utilizing its potentials, can produce the relatively long and large UFG tubes having a simultaneous high strength and good ductility.

**Keywords** Severe plastic deformation · Commercially pure aluminum tube · HTCEC process · Grain refinement · Mechanical properties · Ductility

Today, one of the high-efficiency methods for fabricating ultrafine grained (UFG) and nano-grained (NG) materials which possess superior mechanical properties, are severe plastic deformation (SPD) methods. In SPD processes, an intense plastic strain is applied on the material causing significant grain refinement, and consequently significant improvement of mechanical properties [1]. Some well-known SPD processes used for processing bulk materials

are such as: equal channel angular pressing (ECAP) [2], high-pressure torsion (HPT) [3], cyclic extrusion compression (CEC) [4], cyclic expansion extrusion (CEE) [5], cyclic extrusion channel angular pressing (CECAP) [6] and accumulative roll bonding (ARB) [7]. Some SPD processes such as thinwalled open channel angular pressing (TWOCAP) is developed for U-type cross-sectional shape beams. Moreover, several SPD processes devised for tubular components are such as: tube channel pressing (TCP) [8], tubular channel angular pressing (TCAP) [9, 10], parallel tubular channel angular pressing (PTCAP) [11–14], tube cyclic extrusion compression (TCEC) [15], tube cyclic expansion-extrusion (TCEE) [16], high pressure tube twisting (HPTT) [17] and accumulative spin bonding (ASB) [18]. In TCEC process

✉ G. Faraji  
ghfaraji@ut.ac.ir

<sup>1</sup> School of Mechanical Engineering, College of Engineering, University of Tehran, 11155-4563 Tehran, Iran

of Ref. [15], the initial tube is constrained between chamber and mandrel with a large diameter zone, and also between two end caps. By pressing the mandrel downward, the material of the enclosed tube passes through the neck zone between chamber and mandrel. In this condition, the tube is extruded. After that, the expansion of the pre-extruded material takes place because the material flow is constrained in the die. Thus, TCEC process is a cyclic process in which the material experiences both state of extrusion and expansion. In summary, in TCEC process, tube is kept fixed from outside, but mandrel with a large diameter zone can be moved inside the tube by one hydraulic jack. In HTCEC process introduced in this work, the die design is completely different from that of TCEC process. In HTCEC process, hydraulic fluid is used between the tube and die to eliminate contact friction. Also, unlike TCEC process, a second hydraulic jack is used in HTCEC process which provides adjustable back-pressure.

The main limitation for industrial use of conventional SPD methods such as TCEC is their inability to produce the large and long pieces because in these methods, the further increment of the length and diameter of the piece leads to an intense enhancement of the contact friction between the die and piece, and consequently causes a drastic increase in the required pressing load. In this situation, the buckling or failure of the pressing punch may occur, which is a so dangerous happening. Thus, to dissolve this problem and also to produce the large and long ultrafine grained pieces in SPD methods, the contact friction between the die and piece must be reduced. To achieve this goal, several metal forming techniques have been devised: including, hydrostatic backward extrusion [19], hydrostatic extrusion (HE) [20] and hydrostatic radial forward tube extrusion (HRFTE) [21]. But, the main limitations of these techniques are: first, unlike the SPD methods, the final geometrical dimensions of the processed piece is changed in comparison with the initial condition. Second, unlike the SPD methods, these techniques are unable to apply higher plastic strains to the piece through applying further passes of the process without any changes in the final dimensions of the piece. However, hydrostatic cyclic expansion extrusion (HCEE) [22, 23] and hydrostatic cyclic expansion compression (HCEC) [24] are newly introduced as SPD methods to fabricate long length bulk (rod-shaped) ultrafine grained materials. But, there is still no an efficient SPD method for producing long ultrafine grained tubular-shaped materials, except hydrostatic tube cyclic expansion extrusion (HTCEE) method, which is recently invented by Savarabadi et al. [1]. In HTCEE process, there is nearly no friction between the die and tube which facilitates the production of long UFG tubes. Savarabadi et al. [1] observed that after performing two passes of HTCEE process on commercially pure copper tubes, a significant grain refinement occurred and a UFG microstructure with an

average grain size of  $\sim 127$  nm was formed, while this value was  $\sim 50$   $\mu\text{m}$  for the unprocessed annealed sample. Also, the yield strength, ultimate strength and microhardness was enhanced from 75 MPa, 207 MPa and 59 Hv to 310 MPa, 386 MPa and 143 Hv, respectively. In all SPD methods, the equivalent plastic strain, the shear strain and hydrostatic compressive stress play main roles in grain refinement. A more equivalent plastic strain and shear strain result in more grain refinement, and consequently more mechanical properties improvement. Hydrostatic compressive stress, by enhancing the workability to achieve higher plastic strains before occurring the cracks initiation and propagation, causes a high ductility. Indeed, hydrostatic compressive stresses postpone both stages of crack initiation and crack growth, and also close the cracks and cavities, and prevent the growth of them. Thus, this causes a higher ductility [21, 25, 26]. In this study, hydrostatic cyclic extrusion compression (HTCEC) is introduced as a novel severe plastic deformation method for fabricating the relatively long and large ultrafine grained and nano-grained tubes. In HTCEC process, because of the utilization of pressurized hydraulic fluid between the tube and die, there is nearly no contact friction. This leads to a significant reduction in processing load. Also, the use of movable mandrel placed inside the hollow tube during HTCEC process results in the reduction of the processing hydrostatic pressure. In summary, simultaneous use of the hydraulic fluid and the movable mandrel in HTCEC process facilitates the processing of long and large tubes. Furthermore, unlike HTCEE process [1], a back-pressure system is used in HTCEC process which leads to a significant increase in the amount of hydrostatic compressive stresses; This is the main advantage of HTCEC process over HTCEE process. Higher hydrostatic compressive stresses of HTCEC process, have important advantages such as: first, higher hydrostatic compressive stresses by preventing the crack formation and propagation during the process, facilitate severe plastic deformation of brittle materials. So, in comparison to HTCEE process, HTCEC process is more appropriate for SPD processing brittle materials. Second, in the presence of higher hydrostatic compressive stresses, a higher ductility can be achieved and also a higher number of passes of HTCEC process, and consequently a higher plastic strain can be applied on material leading to more refined microstructure and superior mechanical properties.

In the present study, a novel SPD method named hydrostatic cyclic extrusion compression (HTCEC) process is introduced to fabricate the relatively long and large ultrafine grained and nano-grained tubes. To evaluate the applicability and capability of the HTCEC process, aluminum 5052 alloy tubes were processed by HTCEC up to two passes. Aluminum 5052 alloy is one of the Al-Mg alloys which is mostly utilized in aerospace, marine and automotive industries. This is due to its good formability, high strength

to weight ratio, weldability and corrosion resistance [27]. After applying HTCEC, the microstructure evolution and mechanical properties improvement were examined. To detect the mechanisms of fracture of the tensile testing samples, fractography analysis was performed. Also, finite element method (FEM) is used to investigate the plastic strain and pressing load of HTCEC process.

## 1 Principles of the HTCEC

The sequence of HTCEC process stages is illustrated in Fig. 1a–e. The die setup includes the die, tube, punch, hydraulic fluid, seal, movable mandrel, and back-pressure mandrel. Concerning Fig. 1a, at the start of process, the tube is constrained in HTCEC die using both of the movable mandrel placed inside the hollow tube, and the back-pressure mandrel utilized for applying back pressure. The gap between the tube and die is filled up with hydraulic fluid. Then, this fluid is pressurized by pressing the upper punch on the seal placed between the punch and fluid. Owing to the utilization of pressurized hydraulic fluid between the tube and the die, there is almost no contact friction in this area [1,

22]. This causes a significant reduction in the required pressing load, which facilitates the processing of the long and large tubes. So, HTCEC process has the potential to produce relatively long and large tubes. As seen in Fig. 1, during HTCEC, a movable mandrel is put into the tube, which plays an important role in the reduction of the required hydrostatic pressure. According to Fig. 1b, in the second stage of HTCEC process, the tube is extruded into the deformation zone until the material reaches the back-pressure mandrel which is kept fixed by the lower punch. By continuing extrusion, the material is expanded and then, it fills the hollow region of the deformation zone because of the back pressure role of the back-pressure mandrel. In the third stage, as shown in Fig. 1c, the hydraulic fluid is poured into the outlet channel of die. Then, another seal similar to the upper seal is placed in the outlet channel of die. The hydraulic fluid is pressurized by pressing the lower punch on the lower seal. The back pressure, which is applied by the lower punch, is supplied via another adjustable hydraulic jack system. In the next stage, the movable mandrel and the back-pressure mandrel move together with the tube during the process. As is obvious in Fig. 1d, to continue the process, the upper punch moves downward in the inlet channel. At the same time,

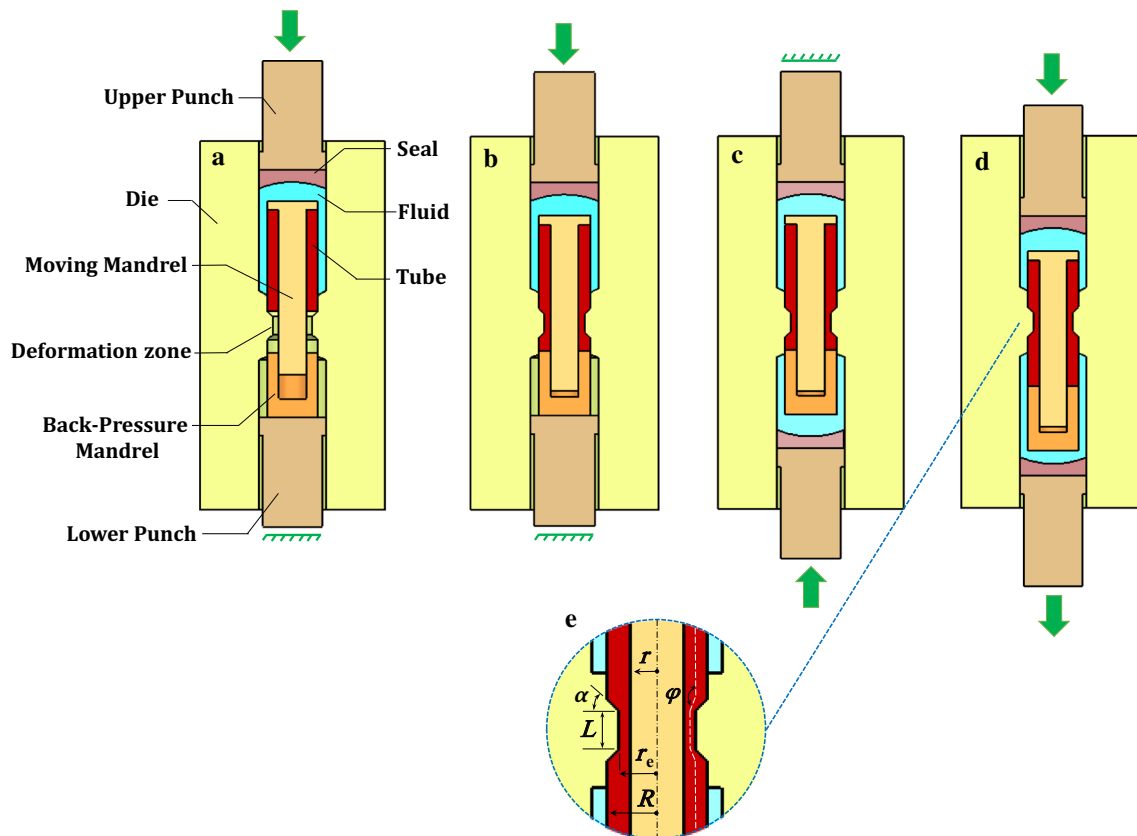


**Fig. 1** Schematic of HTCEC process; **a** at the start of the process, **b** the stage of extrusion followed by expansion in the deformation zone, **c** the utilization of hydraulic fluid and seal in the outlet channel, **d** during the process, and **e** the die parameters

the lower punch is reversed to let the material flow into the outlet channel, and also to keep the strained material in the expanded form. In fact, during HTCEC process, by pressing the upper punch, the lower punch plays a role of back pressure, and leads to continuous expansion of the tube in the deformation zone. So, the dimensions of produced tube in the outlet channel is the same dimensions of the tube in the inlet channel. In other words, HTCEC process does not change the final dimensions of the produced tube compared to those of the initial unprocessed tube. After this stage, one pass of HTCEC process is completed. To perform the second pass of HTCEC, it is enough that the lower punch moves upward in the outlet channel, but this time the upper punch plays the role of back pressure. Subsequent passes of HTCEC can be performed by repeating this cycle to apply an unlimited plastic strain to the material. Another advantage of HTCEC process is that for applying further passes of process, there is no requirement for expelling the tube from the die. The total accumulative equivalent strain of the HTCEC process ( $\epsilon_{HTCEC}$ ) can be calculated from Eq. (1) [15, 16], where  $N$  is the number of passes,  $\phi$  is the include angle ( $\phi \sim 155^\circ$ ). The parameters of Eq. (1) are obvious in Fig. 1e. From Eq. (1), the value of  $\epsilon_{HTCEC}$  for the first and second pass of HTCEC are  $\sim 2.15$  and  $\sim 4.3$ , respectively.

$$\epsilon_{HTCEC} = 2N \left[ \ln \left( \frac{R^2 - r^2}{r_e^2 - r^2} \right) + \frac{4}{\sqrt{3}} \cot \left( \frac{\phi}{2} \right) \right] \quad (1)$$

## 2 Experimental and FEM Procedures

In this study, tubes of aluminum 5052 alloy with a chemical composition mentioned in Table 1, were processed by HTCEC process through two passes at room temperature. Tubes with a length of 100 mm and an outer diameter of 20 mm, and a thickness of 2.5 mm were prepared by machining. The annealing was carried out by subjecting the samples to a temperature of 500 °C for 1 h, then cooling in air [28]. The HTCEC die and its parts (Fig. 1a) were manufactured from hot-worked tool steel and hardened to  $\sim 55$  HRC. The values of the die parameters indicated in Fig. 1e are as follows:  $r = 7.5$  mm,  $R = 10$  mm,  $r_e = 9$  mm,  $L = 7$  mm and  $\alpha = 45^\circ$ . The HTCEC equipment, the die and its components are illustrated in Fig. 2. The pictures of unprocessed tube and the HTCEC processed tubes are indicated in Fig. 3. In this

process, hydraulic oil was used as a pressurized fluid. Also, the channels of die are sealed using pieces of polytetrafluoroethylene (PTFE) with a diameter a bit larger than channels one. The PTFE pieces are squeezed in the channels to prevent the hydraulic fluid from leaking. A hydraulic press machine and a hydraulic jack system are used for applying pressure and back pressure to the material, respectively. The process was done at a ram speed of about 5 mm/min. Tensile properties, such as strength and ductility, of the unprocessed and the HTCEC processed tubes were evaluated using the tensile tests at room temperature at a strain rate of  $10^{-3} \text{ s}^{-1}$ . The tensile testing samples with a gauge length of 6 mm, a gauge width of 3 mm and a thickness of 2.5 mm were prepared along the tube axis by wire EDM machining. After tensile testing, to determine the mechanisms of fracture, field emission scanning electron microscopy (FESEM) model FEI Nova NanoSEM 450 was employed at a voltage of 10–15 kV. Microhardness of the tubes was evaluated at a cross section perpendicular to the tube axis using Wolpert testing machine type V-Testor 2 at a load of 100 g and a stop time of 10 s. General standard metallography and optical microscopy (OM) were utilized to study the microstructure of the tubes. Modified Poulton's reagent was used for etching the polished specimens to obtain the OM microstructure [29]. The OM evaluations were done in the cross section perpendicular to the tube axis. Also, the microstructure of the HTCEC processed tubes were scrutinized by transmission electron microscopy (TEM). For TEM characterization, the disc shaped samples were punched from the regions near the outer surface of tubes. Then, electro-polishing in a solution of 33% nitric acid and 67% methanol as an etchant was done to provide the specimens for TEM studies. Finally, TEM images are taken by transmission electron microscope model FEI Tecnai G2 F20 operating at 200 kV. The finite element (FEM) simulation of HTCEC process were employed using Abaqus/Explicit software to study the deformation behavior, equivalent plastic strain, and required pressing load. The process was simulated in the form of a 2D axisymmetric model, and the whole of the tube model was meshed using a number of 1000 of CAX4R linear quadrilateral elements with 1206 nodes. The edge length of the used square elements was 0.5 mm. The tube was modeled as a deformable piece, and the components of the die were modeled as rigid bodies. In the simulation, the geometrical dimensions of the tube and die components and also the mechanical properties of the tube were considered as the same as the real values. Adaptive meshing method, which is an automatic

**Table 1** Chemical composition of the AA5052 alloy used in this study (wt%)

Specimens	Elements							
	AL	Mg	Fe	Si	Mn	Cr	Cu	Zn
AA5052 alloy	Base	2.48	0.26	0.14	0.10	0.18	0.01	Trace

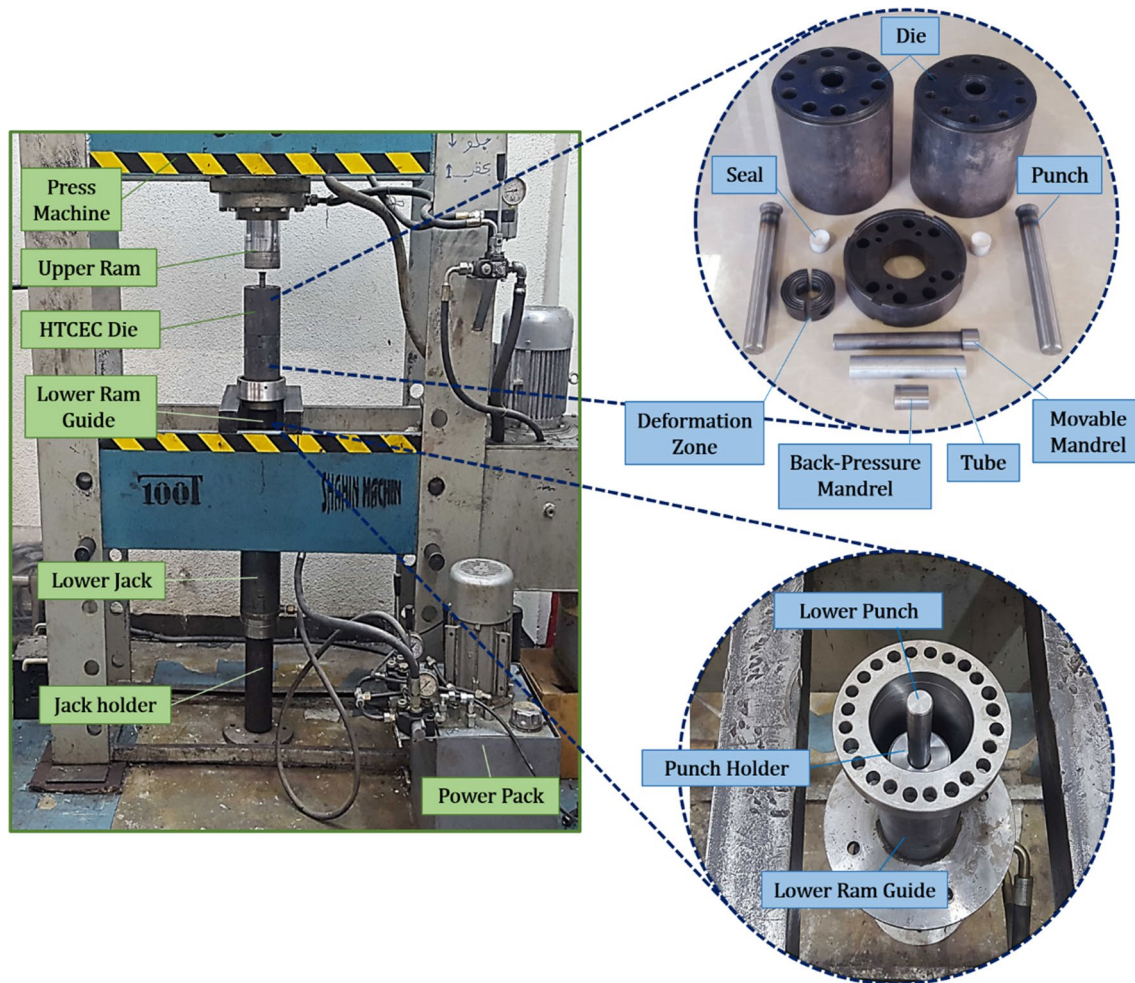


Fig. 2 The HTCEC process equipment, the HTCEC die and its components



Fig. 3 The pictures of the unprocessed tube and the HTCEC processed tubes

remeshing technique, was utilized to adapt the larger plastic strains and also to enhance the accuracy of the results

[21]. In deformation zone, where there is a physical contact between the tube and die, the Coulomb friction coefficient was considered to be 0.05 [21]. But, the contact between the channels of die and the tube is considered frictionless because of the presence of pressurized hydraulic fluid in these areas [1, 22].

### 3 Results and Discussion

#### 3.1 Microstructure Evolution

Figure 4 shows the OM microstructure of the unprocessed tube in the center of the tube thickness in the cross section perpendicular to the tube axis. As shown, the initial microstructure contains nearly equiaxed coarse grains with an average grain size of  $\sim 360 \mu\text{m}$ . The impurity phase particles are also obvious on the grains. Figure 5 indicates the TEM microstructure of the tube after the first and second pass of HTCEC process. As seen, after the first pass of HTCEC,

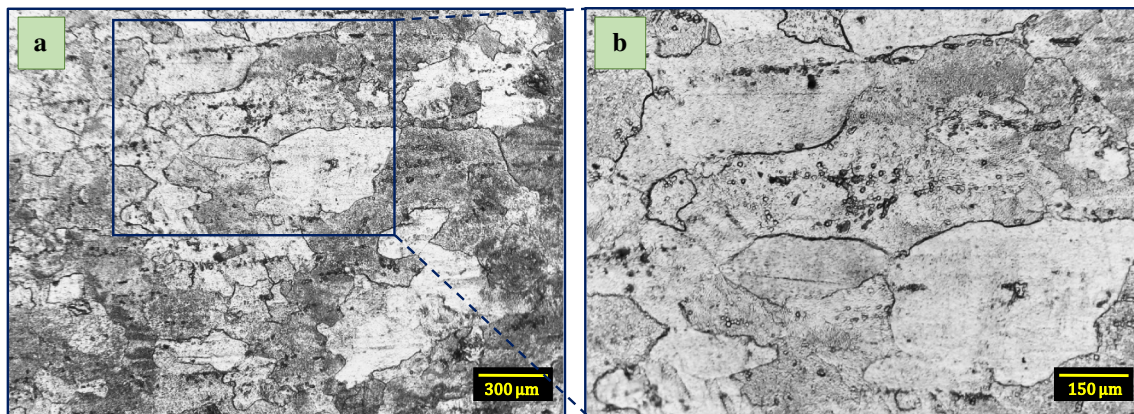


Fig. 4 The OM microstructure of the unprocessed at two magnifications **a**, **b**

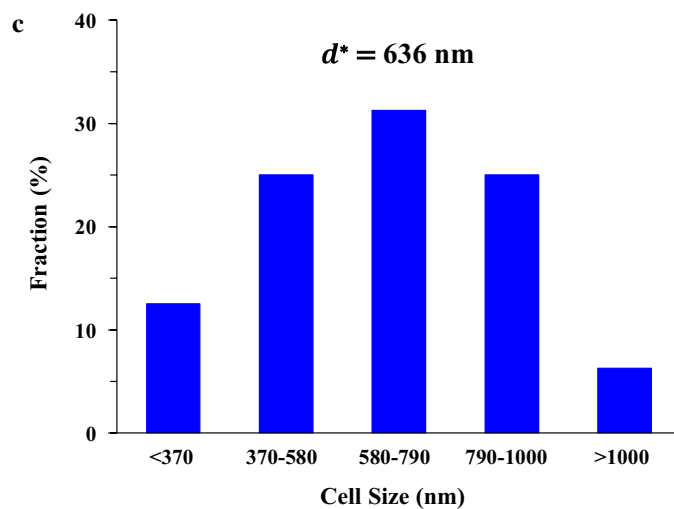
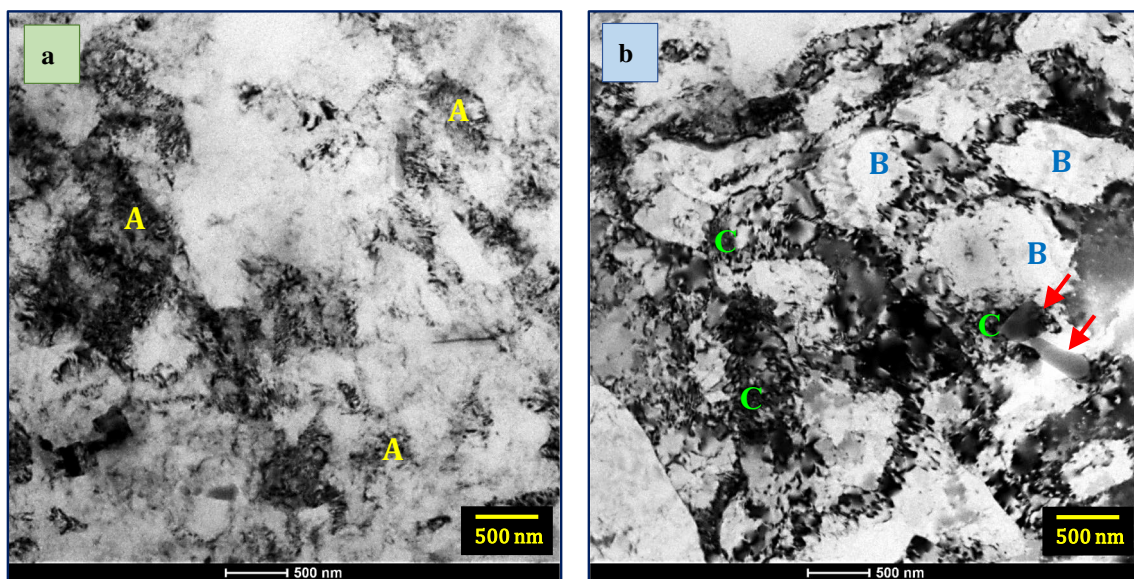


Fig. 5 The TEM microstructure of the tube after the first pass **a** and second pass **b** of HTCEC process, and **c** the histogram of the cell size distribution of **b**

tangled and diffused arrangements of dislocations (marked as A) are formed, and the grain size is exceedingly reduced and ultrafine cells are created. In other words, intense plastic straining, mostly due to consecutive shear straining during HTCEC process, causes the significant enhancement of dislocation density and formation of severely tangled dislocation structures (marked as A). From Fig. 5b, by applying more strain to material through performing two passes of HTCEC, dislocations are rearranged into low angle grain boundaries (LAGBs), and subsequently into dislocation cells, to reduce the strain energy and form boundaries of the cells. Thus, a cellular structure (marked as B) is appeared in which the cell boundaries are chiefly formed from dislocations in the tangled configuration or a high density of disordered dislocation clusters (marked as C). In this condition, it was reported that compared to the cells interiors, a higher density of dislocations can exist at the cells/subgrains boundaries [30, 31]. The dislocation cells are low energy structures which are typically appeared during the plastic deformation of metals with medium to high stacking fault energy [32]. Concerning Fig. 5b, In comparison to the microstructure of the unprocessed tube (Fig. 4) and that of the one-pass HTCEC processed tube as shown in Fig. 5a, a more refined, more homogeneous and more equiaxed sub-micrometer ultra-fine cell/subgrain microstructure with an average size of ~636 nm is formed in the two-pass HTCEC processed tube. The histogram of the cell size distribution of the two-pass tube are illustrated in Fig. 5c. In general, ultra-fine cells/subgrains (marked as B) divided by dislocations tangles and clusters (marked as C) are obvious in Fig. 5b. But, because of the presence of many disordered tangled dislocations (marked as A) within the microstructure of the one-pass tube, see Fig. 5a, such a cell structure of the two-pass tube are not well developed. In fact, Fig. 5a contains many small subgrains with poorly defined boundaries. By increasing the imposed plastic strain, tangled dislocations can move to the subgrains boundaries or can form new boundaries to create small subgrains from large ones [33]. In other words, at low strains, tangled and diffused arrays of dislocations are formed, and by increasing strain, the majority of dislocations create the boundaries of subgrains or cells, as reported in other studies such as Ref. [34]. In this condition, by increasing strain, a higher density of dislocations will accumulate at the subgrains boundaries, and high-angle grain boundaries (HAGBs) will be developed. The higher number of SPD passes can lead to the reduction of dislocations density in the grain interiors. This can be as a result of: (a) dynamic recovery causing a balance between the creation and annihilation of dislocations; and (b) dislocations movement from subgrains interior to their existing boundaries to create grains [33, 35, 36]. Also, according to Fig. 5, the finer second phase particles are obvious within the Al-matrix. In fact, under the effect of shear strain

induced by SPD processes, the initial phase particles of the annealed alloy can be broken to smaller sizes. These finer particles have an important role in controlling the mechanical properties of the material because of promoting dislocation accumulation through pinning of dislocations. The fine precipitates are indicated by red arrows in Fig. 5b. During SPD processing of metals and alloys, three parameters of equivalent plastic strain, shear strain and hydrostatic compressive stress play main roles in the occurrence of grain refinement. In this way, further equivalent plastic strain and shear strain causes more grain refinement. Concerning Fig. 5, by applying subsequent passes of SPD process, and consequently applying further shear strain to the material, the level of grain refinement and the homogeneity of microstructure can be enhanced, as also seen in Refs. [1, 2, 11, 12], and a higher density of dislocations is produced [37–40]. Also, it is observed that further SPD passes can lead to a more equiaxed ultra-fine grains [41–45].

From this study and previous related studies, the grain refinement of aluminum 5052 alloy subjected to HTCEC is postulated as follows: At the early stages of applying SPD methods, the density of dislocations increases and then, the dislocations start to interact with each other and form the dislocation tangles and the arrangements of dislocations inside the primary large grains. This leads to the formation of dislocation cells which are an intragranular structures with low angle misorientation and boundaries [33, 35, 46]. So, a microstructure with two regions of low and high density of dislocations is formed. With increased straining, the dislocations density increases and the cell size becomes finer [47, 48]. By continuing the deformation, a high number of dislocations are accumulated in the cell walls, which can lead to the generation of subgrains with low angle boundaries [47]. The continuation of process results in the increment of the number of subgrains. When the material passes through the shearing zones of the die, particularly during a higher number of passes, the subgrains experience rotations relative to each other, the increment of misorientation due to the increased density of dislocations in the subgrain boundaries, and the grain fragmentation [33, 49, 50]. In fact, because of this misorientation phenomenon, low angle boundaries are gradually converted into the high angle ones, leading to the creation of arrays of ultrafine grains separated by high-angle grain boundaries. In this way, an ultrafine-grained (UFG) microstructure is formed after SPD process. By contrast, this microstructure evolution cannot be achieved in most conventional metal forming techniques because of their natural limit for applying higher total plastic strains [51]. From previous studies [52–55] it is found that by increasing the number of passes of SPD processes, the fraction of high angle grain boundaries is increased. This is caused by the increment of subgrains rotation due to the accumulated strain, the increment of subgrains misorientation due to the

absorption of dislocations at boundaries, and also the influence of shear strains [15, 55, 56]. Also, at higher number of SPD passes, coarse cells are subdivided to the equiaxed smaller ones having well-defined and sharp boundaries.

### 3.2 Mechanical Properties

Figure 6 shows the room temperature engineering stress–strain curves of the unprocessed tube, the one-pass, and two-pass HTCEC processed tubes. The important tensile properties obtained from Fig. 6a is represented in Fig. 6b. As seen in Fig. 6, after applying the first pass of HTCEC, the yield strength, ultimate strength, uniform elongation and elongation to failure have reached to 206 MPa, 252 MPa, 10.4, and 19.4%, respectively while these values for the unprocessed tube are 98 MPa, 178 MPa, 23.2%, and 31.6%, respectively. The enhancement of strength after applying SPD processes is a common phenomenon which was also reported in numerous studies such as Refs. [1, 2, 11, 12]. Concerning Fig. 6, two passes of HTCEC leads to further enhancement of strength. In this observation, the yield strength, ultimate strength, uniform elongation and elongation to failure of the two-pass tube have reached to 254 MPa, 306 MPa, 8.8, and 15.4%, respectively. The enhancement of strength after applying HTCEC process can be as a result of: (a) strain hardening: during the initial passes of process, a higher density of dislocations is produced, which results in a significant strain hardening. This is a main reason for increasing strength and decreasing elongation in initial passes. (b) Grain boundary strengthening: as mentioned earlier, by continuing SPD process, particularly in higher number of passes, the gradual reduction of the grains size and the formation of nanostructured subgrains and ultrafine grains takes place, which leads to significant increment of the strength [48]. It is because that the grain boundaries play a role of an obstacle on the path of dislocations movement,

causing the enhancement of the material resistance to deformation and consequently, the enhancement of strength [57]. Also, Hall–Petch equation for strength demonstrates that by reducing the material grain size, strength increases [58]; and (c) Particle strengthening: as seen in Fig. 5, the strain imposed by HTCEC process can cause breaking impurity phase particles, and consequently the formation of more finer and more homogenous particles which prevent the dislocation movement. So, this leads to the enhancement of the material strength. Concerning Fig. 6, during tensile tests, a lower strain hardening are observed in the stress–strain curves of the HTCEC processed tubes compared to that of the unprocessed tube. This is one of the remarkable features of the deformation behavior of UFG materials [59]. The reason for this observation can be the absorption of dislocations into the grain boundaries, as an effective recovery process [54].

For the two-pass HTCEC processed tube (Fig. 6), an increased strength is achieved without a considerable ductility drop compared to the ductility value of the one-pass tube. This is be due to the formation of a more refined and more homogeneous microstructure with nearly equiaxed grains and a higher fraction of high-angle grain boundaries. The comparisons of the elongation to failure, ultimate tensile strength, uniform elongation and hardness of the HTCEC processed tubes with the results of other studies performed on 5052 Al alloy, such as: 2, 4 and 6 passes Equal channel angular pressing (ECAP) [27], 1 and 2 passes Constrained groove pressing (CGP) [30], 1 and 2 passes CGP [60], 2, 4 and 6 passes ECAP [28, 61], 90% Cryo groove rolling followed by Warm rolling (CGW) [29], 33 and 87% Cold Rolling (CR) [62], 4 passes Differential speed rolling (DSR) [31], 5 passes Accumulative roll bonding (ARB) [63], and 4 and 8 passes ECAP [64], are illustrated in Fig. 7. As seen, in comparison to other processes, the HTCEC processed tubes possess considerably higher values of the elongation

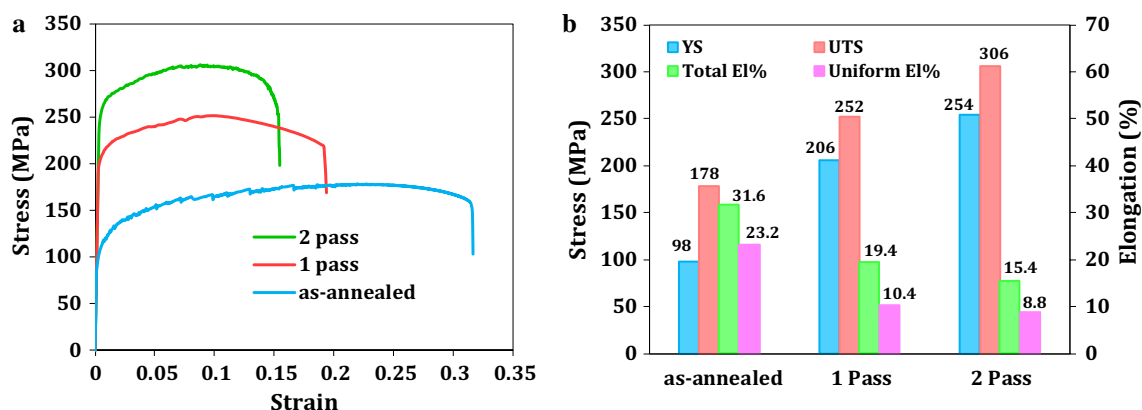


**Fig. 6** **a** Engineering stress–strain curves of the unprocessed tube, the one-pass, and two-pass HTCEC processed tubes, and **b** the important tensile properties obtained from tensile curves



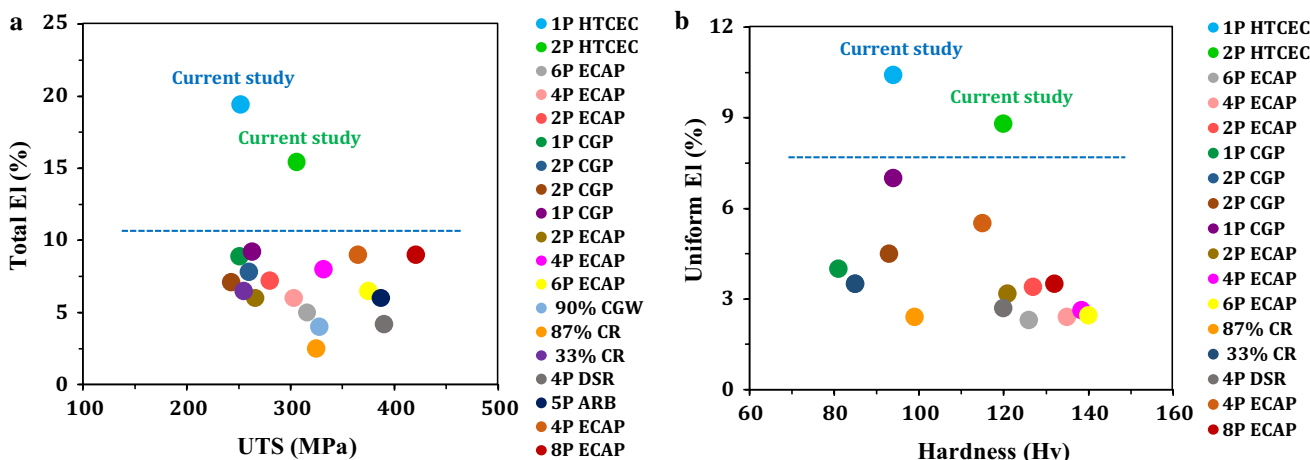


Fig. 7 Comparison of the a elongation to failure (Total El) and ultimate tensile strength (UTS), and b uniform elongation (Uniform El) and hardness of the HTCEC processed tubes with the results of other studies performed on 5052 Al alloy

to failure and uniform elongation beside high values of the ultimate tensile strength and hardness (especially the two-pass HTCEC processed sample). Thus, the HTCEC process has the potential to produce the tubes with simultaneous high strength and good ductility. This feature is one of the main advantages of the HTCEC process because a combination of high strength and high ductility is very noteworthy for the practical and industrial applications of the material. The utilization of this ideal material leads to prevention of catastrophic failure of piece during service. This feature of HTCEC process is mostly attributed to the existence of higher hydrostatic compressive stress in HTCEC process (as discussed in the simulation results section). In addition to the equivalent plastic strain which is an important factor in SPD processes, the hydrostatic compressive stress and shear strain play main roles in producing ultrafine-grained and nano-grained materials [65]. Hydrostatic compressive

stresses by delaying the crack initiation and propagation, and also by closing the cracks and small defects or by restricting their growth, lead to a better ductility [21].

The results of Vickers microhardness measurements of the unprocessed tube, the one-pass, and two-pass HTCEC processed tubes along the tube thickness (path A–B) are demonstrated in Fig. 8a, and the average value of the results of Fig. 8a are represented in Fig. 8b. As seen, after processing by HTCEC or by increasing the number of pass, the microhardness value is increased.

Also, the value of microhardness increases from the inner surface to the outer surface of the tube along the thickness. This trend is in agreement with the distribution of equivalent plastic strain along the tube thickness represented in Sect. 4.4. In fact, the increment of microhardness along the tube thickness is related to applying higher plastic strain to the outer surfaces of the tube during HTCEC process. The

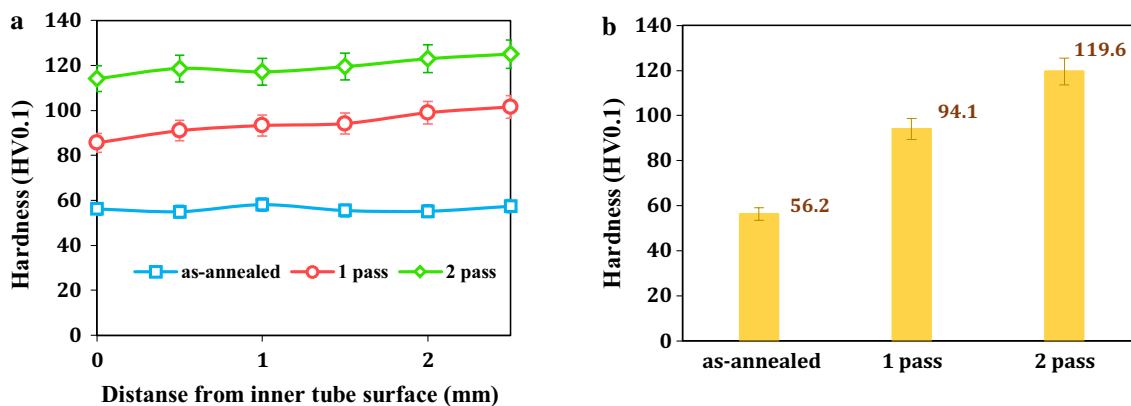


Fig. 8 a Micro-hardness distribution along the tubes thickness for the unprocessed tube, the one-pass, and two-pass HTCEC processed tubes, and b the average values of the results of a

enhancement of hardness after applying SPD techniques is a common event which is also seen in many studies such as Refs. [1, 2, 11, 12]. This is related to the grain refinement, enhancement of the amount of grain boundaries, enhancement of the density of dislocations, work hardening occurred during the plastic deformation, and the distribution of the second phase finer precipitations. Also, Hall–Petch equation for hardness denotes that the reduction of grain size results in the enhancement of hardness [66]. Concerning Fig. 8, the maximum value of microhardness ( $\sim 120$  Hv) is achieved for the two-pass HTCEC processed tube which possesses the most refined microstructure (as illustrated in Fig. 5), while the microhardness value of the unprocessed tube is only  $\sim 56$  Hv. Also, it is observed that after applying the first pass of HTCEC, the microhardness value is increased abruptly from 56 HV to 94 HV. The suddenly increment of strength after the first pass of SPD processes can be attributed to the fast production and accumulation of a high density of dislocations and consequent dislocation hardening. According to Fig. 8a, by increasing the number of pass, the homogeneity of microhardness distribution through the thickness is enhanced. Thus, a homogeneous properties through the thickness is expected in higher passes of HTCEC. This feature is another advantage of the HTCEC process. In this way, as seen in Fig. 8a, In comparison to one pass, two passes of HTCEC led to a better uniformity of microhardness. Also, it is observed in Fig. 8a that by increasing the number of HTCEC passes, hardness values tends to reach a saturation level. Similar saturation trend was also seen in other studies such as Refs. [1, 2, 11, 44, 67]. One main reason for this observation can be the establishment of a dynamic balance between the creation of dislocations and the annihilation related to the dynamic recovery process, at higher passes of SPD processes [68]. In other words, at higher number of passes, the role of dislocation density in strengthening is reduced whilst the role of the grain boundaries remains nearly constant. Thus, the hardness and yield stress reach a saturation level [54]. As mentioned before, Fig. 7b exhibits the comparison of the hardness of the HTCEC processed tubes with that of other studies. As is obvious, the HTCEC processed tubes, especially the two-pass tube, possess considerably high hardness values.

### 3.3 Fractography

The fracture surfaces of tensile specimens prepared from the unprocessed tube, the one-pass, and the two-pass HTCEC processed tubes, are shown in Fig. 9. As is obvious, the dimples existed in the fracture surface of the unprocessed sample are generally equiaxed, large and deep, which is typically attributed to ductile fracture behaviour [33, 69]. Also, these features are indicative of higher formability of the unprocessed tube compared to that of the HTCEC processed tubes.

According to Fig. 9, by increasing the number of HTCEC passes, and consequently by applying more strain to the material, smaller and shallower dimples are formed. The appearance of small and shallow dimples after tensile testing of the SPD processed samples is also seen in other studies [1, 2, 11, 12, 67]. The decrease in the dimple size is related to grain refinement and work hardening happened during SPD process [69, 70]. Also, as it is clear from the results of tensile tests, further passes of HTCEC process leads to the enhancement of strength and the reduction of elongation. Thus, by increasing the number of HTCEC passes, the plastic deformation is reduced, and dimples don't have enough time to grow and coalescence with one another, helping to the formation of shallower and smaller dimples on the fracture surface. According to Fig. 9, the fracture surface of the two-pass HTCEC processed specimen contains the smallest and shallowest dimples among all specimens, and also contains a higher amount of sharp tearing edges (the white arrows shown in Fig. 9). This can be indicative of a common feature of ductile fracture which is mainly associated with the creation of many dimples and microcavities during the plastic deformation instead of significant growing of the previously formed small dimples and microcavities [71, 72]. Also, the existing intermetallic phases at the grain boundaries, as a kind of defect, are appropriate for crack nucleation and propagation. It is because that these phases cut off the continuity of Al matrix, so they induce stress concentration and lead to micro-cracks initiation [72]. The ultra-fine grained (UFG) structure can hinder the crack propagation by blunting or delamination mechanisms [30]. Also, the homogeneous dispersion of the particles of intermetallic phases in Al matrix can contribute to limiting micro-cracks propagation. In this condition, intermetallic particles play a reinforcing role in inhibiting crack growth [72]. Overall, the fracture trend of the specimens of Fig. 9 is as follows: the creation of microvoids, their subsequent growth and coalescence with one another to form crack. Then, the crack grows, leading to fracture. This fracture trend denotes ductile fracture mode [1, 33]. So, it is claimed that mainly ductile fracture happened in all specimens. However, there are some indications of brittle fracture in the two-pass HTCEC processed specimen. It seems that further passes of HTCEC can result in predominantly brittle fracture.

### 3.4 Simulation results

Figure 10 shows the FEM calculated force–displacement diagrams of the first pass of HTCEC process (with  $\mu=0$ ) and frictional TCEC process (with  $\mu=0.1$ ) for two different lengths of tube. According to Fig. 10 the maximum force required for HTCEC processing 100 mm tube is only 78 kN while this value for frictional TCEC is  $\sim 815$  kN ( $\sim 10.45$  time higher). Also, concerning Fig. 10 the maximum force

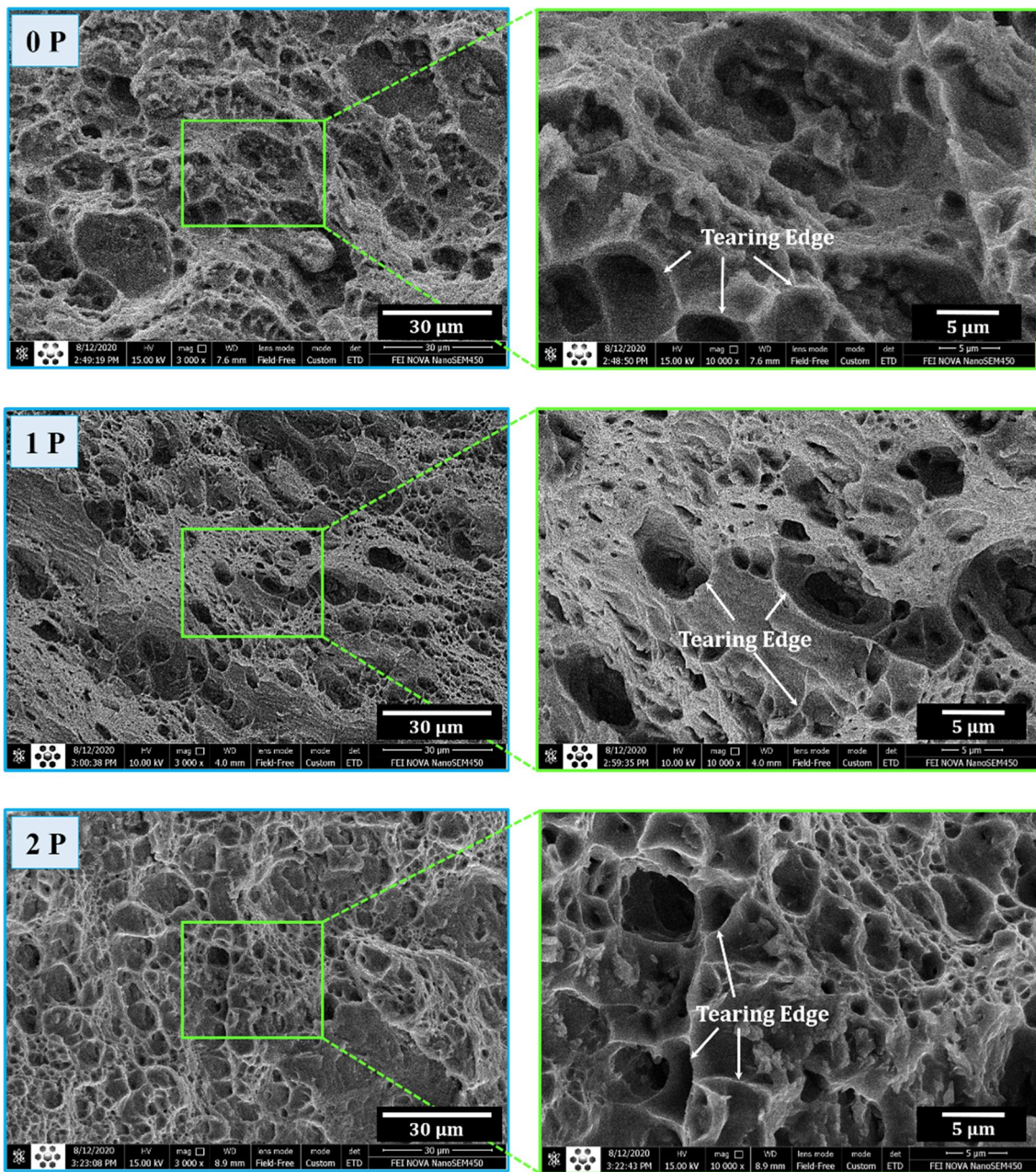


**Fig. 9** The SEM micrographs taken from the fracture surfaces of the tensile specimens extracted from the unprocessed tube, the one-pass, and the two-pass HTCEC processed tubes

required for HTCEC processing 200 mm tube is only ~80 kN (nearly the same amount recorded for 100 mm tube), but this value for frictional TCEC is ~1310 kN (~16.37 time higher). In general, the significantly lower required force of HTCEC process is related to the elimination of friction force between the die and tube because of using pressurized hydraulic fluid [21, 22]. Two important conclusions which can be drawn from the diagrams of Fig. 10, are as follows: (a) the required force of HTCEC process is significantly lower than that of frictional TCEC process. (b) HTCEC

process is independent of the length of the tube because, as seen in Fig. 10, the increment of the tube length don't lead to a significant change in the required force of HTCEC process. Therefore, it is claimed that the HTCEC process can be used for production of long length UFG tubes having higher mechanical properties. The reason for the appearance of fluctuations in the diagrams of Fig. 10 is the occurrence of discontinuous contact between the tube and die during FEM analysis [22]. During applying SPD processes, especially at industrial scale, the buckling and fracture of punch

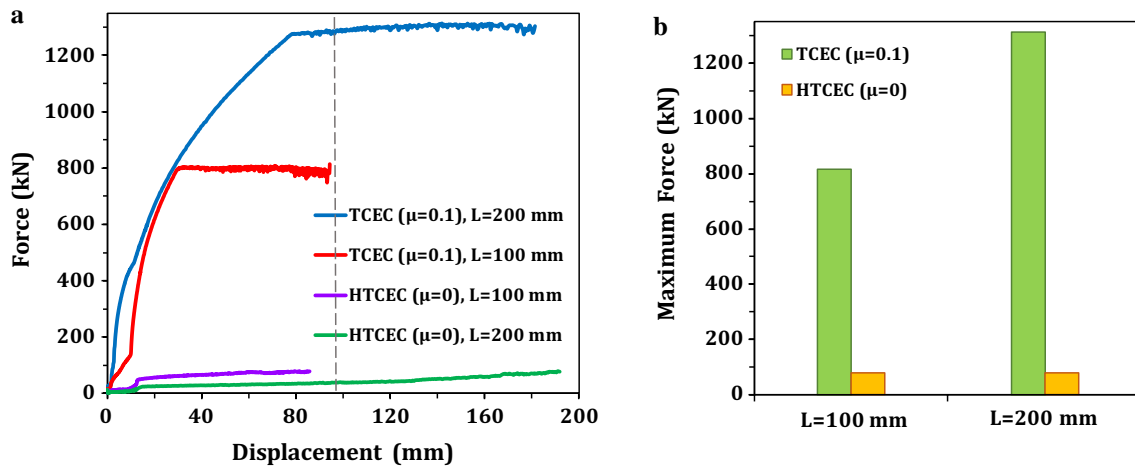


**Fig. 10** **a** the diagrams of required force–ram displacement obtained from FEM for the first pass of HTCEC process ( $\mu=0$ ) and frictional TCEC process ( $\mu=0.1$ ) for two different tube lengths of 100 mm and 200 mm. **b** the comparison of maximum forces obtained from **a**

is not economical, and also it is dangerous for the operator health. Another advantage of the HTCEC process over the frictional TCEC process is that there is a significantly lower risk of punch buckling in HTCEC process. As known, for an ideal straight column, the critical force of buckling ( $P_{cr}$ ) is calculated using the following formula:  $P_{cr} = (\pi^2 EI)/L_e^2$ , where  $E$  is Young's modulus,  $I$  is the second moment of area and  $L_e$  is the beam effective length. For a steel punch with cylindrical geometry with a Young's modulus of 200 GPa, a radius of 10 mm and a length of 200 mm, the amount of  $P_{cr}$  is calculated  $\sim 790$  kN. In this calculation, it is assumed that  $L_e = 0.7 L = 140$  mm ( $L$  is the punch length) because of considering the condition of one pinned end, and one fixed end. The calculated  $P_{cr}$  (790 kN) is significantly lower than the required force of the frictional TCEC process ( $\sim 1310$  kN from Fig. 10), but this amount of  $P_{cr}$  (790 kN) is higher than the required force of HTCEC process ( $\sim 80$  kN from Fig. 10). It means that processing of a tube with a length of 200 mm by frictional TCEC process leads to buckling and failure of the punch. Thus, the frictional TCEC process cannot be used for production of long tubes. But, HTCEC process is a good choice for production of long tubes without the risk of punch buckling and failure because of its lower required force.

Figure 11 shows the distribution of equivalent plastic strain for the HTCEC processed tube at the different stages of deformation from the beginning of process until the end of the second pass. From Fig. 11, a non-uniform distribution of equivalent plastic strain is observed through the tube thickness. In this way, the outer surfaces of the tube shows higher plastic strains. The inhomogeneous distribution of plastic strain leads to the inhomogeneous distribution of microhardness through the tube thickness, which is obvious in Fig. 8a. For having a better outlook, the diagrams of equivalent plastic strain variation along

the thickness (path A–B) during the first and second pass of HTCEC process are illustrated in Fig. 12. Also, the local deformation history of six probe points (named P1 to P6) located through the tube thickness are indicated in Fig. 13. According to Figs. 12 and 13, the distribution of equivalent strain along the tube axis is nearly uniform in each pass of HTCEC, but it is non-uniform along the thickness. In this way, the outer surfaces of the tube experience higher equivalent plastic strain compared to the inner ones because of the material deformation pattern during processing by HTCEC. Concerning Fig. 12, one pass of HTCEC leads to a variation in equivalent strain from  $\sim 1.5$  to  $\sim 2.75$  along the thickness (path A–B), and two passes of HTCEC cause a strain variation from  $\sim 3.25$  to  $\sim 5$ . As seen in Fig. 13, by applying each pass of HTCEC, each probe point experiences a certain history of strain. Two significant strain mutations observed in all diagrams of Fig. 13 are related to the passing of the material through the deformation zone of the die during each pass of HTCEC. According to Fig. 12, the average equivalent plastic strain across the tube thickness for one and two passes of HTCEC process obtained from FEM analysis are 2.07 and 4.03, respectively, which are relatively near the theoretical values of 2.15 and 4.3 calculated by Eq. (1). From this comparison, it is found that the FEM model of this study exhibits the distribution of equivalent plastic strain with an acceptable accuracy. Figure 14 indicates the distribution of hydrostatic compressive stress in the HTCEC processed tube. As seen, higher hydrostatic compressive stress exists in HTCEC, leading to the increment of the material ductility (as explained before). The amount of hydrostatic compressive stress of HTCEC is considerably higher than the most of the other SPD techniques such as CECAP and ECAP [73]

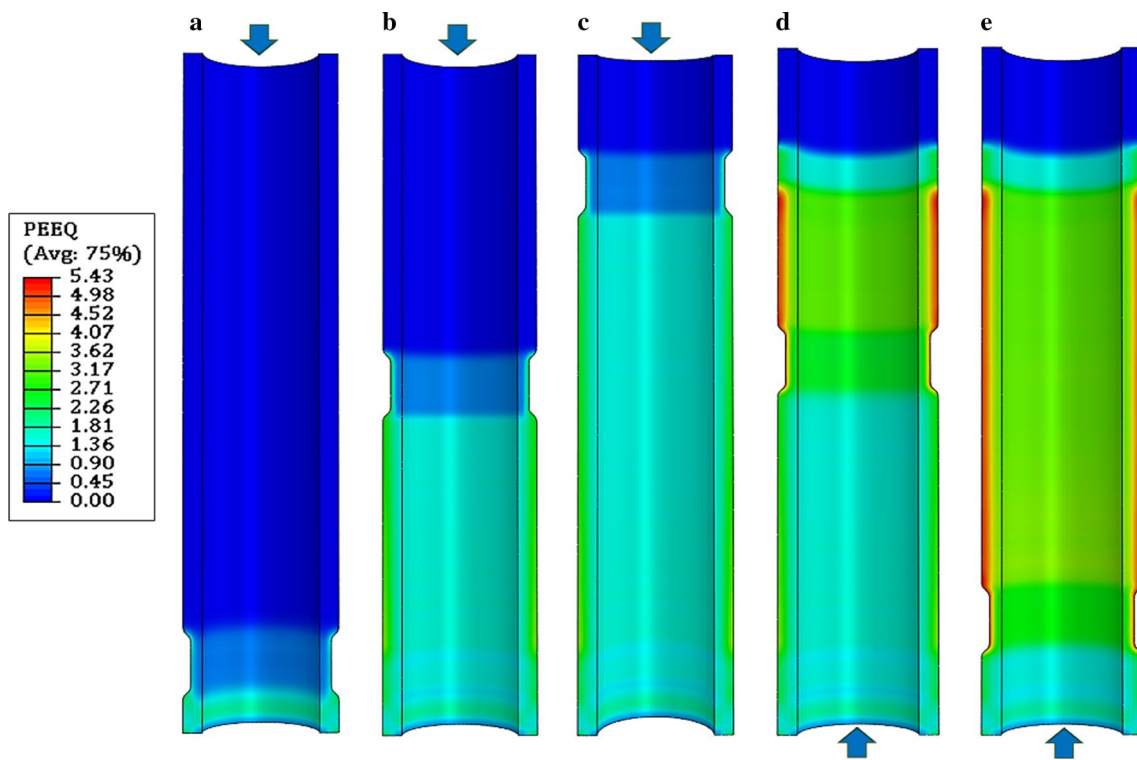


Fig. 11 The contours of equivalent plastic strain at different stages of deformation during the first pass a–c and the second pass d–e of HTCEC process

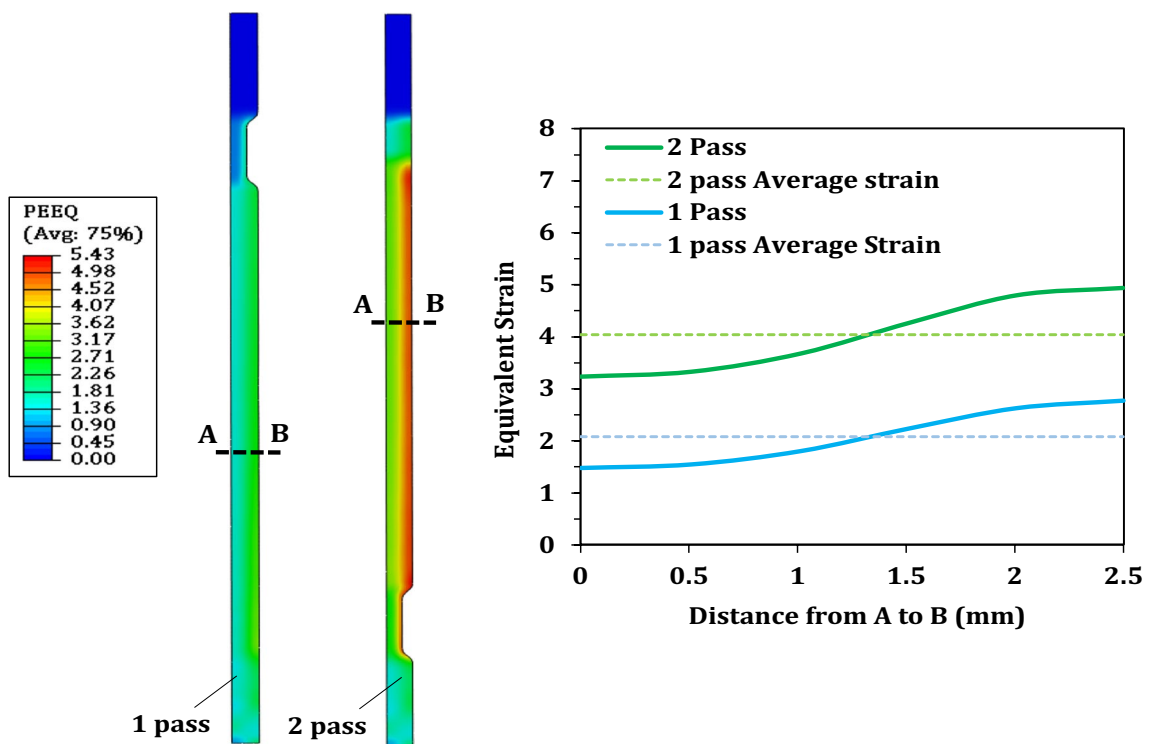
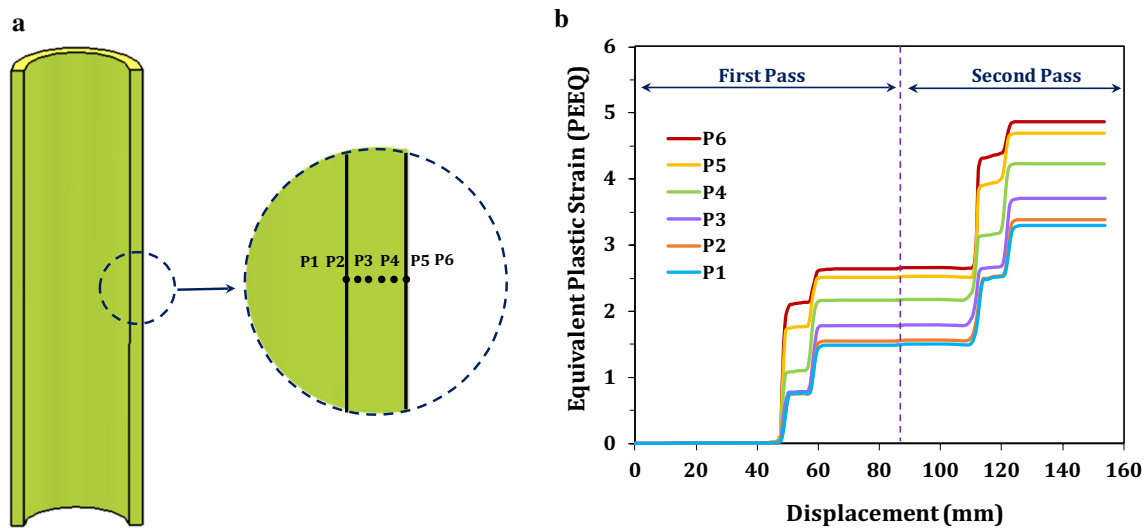
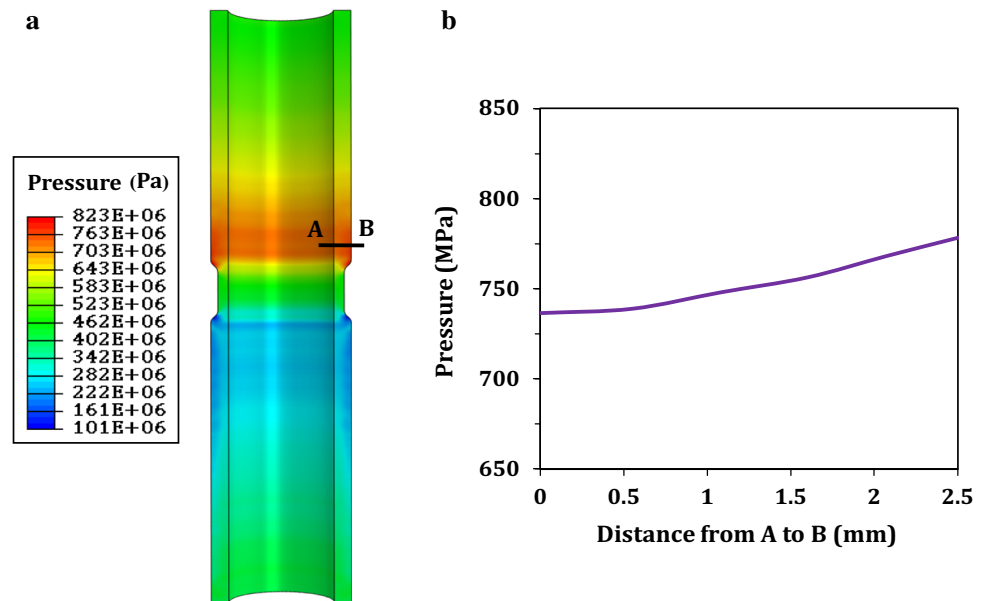


Fig. 12 The diagrams of equivalent plastic strain variation along the thickness (or along path A–B) during the first and second pass of HTCEC process



**Fig. 13** **a** six probe points located on the tube thickness and **b** The diagrams of equivalent plastic strain versus ram displacement during HTCEC process at the points.

**Fig. 14** **a** The contours of hydrostatic pressure during HTCEC process. **b** hydrostatic pressure distribution along the thickness (or along path A–B)



## 4 Conclusions

In this study, hydrostatic cyclic extrusion compression (HTCEC) is introduced as a novel severe plastic deformation technique for production of the relatively long and large ultrafine grained (UFG) and nano-grained (NG) tubes. Aluminum 5052 alloy tubes were processed by HTCEC up to two passes. Then, the microstructure evolution and mechanical characteristics of tubes were investigated. Fractography analysis was done to distinguish the mechanisms of fracture. Also, the FEM is used to investigate the effects of HTCEC process on plastic strain

and pressing load. Ultimately, the following results were obtained from this study:

- HTCEC process is an appropriate technique for producing relatively long and large ultrafine grained and nano-grained tubes which possess superior mechanical properties. This is attributed to the fact that in HTCEC, the pressing load is almost independent of the tube length. It is because that the use of the pressurized hydraulic fluid between the tube and die leads to the elimination of contact friction.
- HTCEC process requires significantly lower pressing load in comparison with the frictional TCEC process.

- Two passes of HTCEC led to the formation of a more refined and more homogeneous ultra-fine subgrains microstructure with an average cell/subgrain size of ~636 nm while the average grain size of the unprocessed sample was ~360  $\mu\text{m}$ .
- HTCEC process has the potential to produce a material with a combination of higher strength and good ductility. In this way, two passes of HTCEC led to a notable increase in: (a) the yield strength by ~260% from 98 MPa to 254 MPa, (b) the ultimate strength by ~172% from 178 MPa to 306 MPa, and (c) the microhardness by ~214% from ~56 Hv to ~120 Hv. Simultaneously, a drop of ductility from 31.6 to 15.4% took place, which is lower than that reported in other studies. In other words, a good combination of high strength and sufficient ductility was achieved from the HTCEC process compared to other studies. This is mainly related to the presence of higher hydrostatic compressive stresses in HTCEC process (as illustrated in the simulation section).
- Fractography analysis showed that the fracture is caused by ductile fracture as a dominant mechanism of fracture, although some indications of brittle fracture in the two-pass HTCEC processed specimen was detected.
- One pass of HTCEC process caused the variation of equivalent strain from ~1.5 to ~2.75 along the thickness. This variation for two passes of HTCEC was from ~3.25 to ~5. The average values of equivalent strain for both number of passes were near the theoretical values.

**Acknowledgements** This work was supported by Iran National Science Foundation (INSF).

## References

1. M.M. Savarabadi, G. Faraji, M. Eftekhari, *Met. Mater. Int.* **27**, 1686 (2021)
2. M. Eftekhari, G. Faraji, S. Nikbakht, R. Rashed, R. Sharifzadeh, R. Hildyard, M. Mohammadpour, *Mater. Sci. Eng. A* **703**, 551 (2017)
3. A. Al-Zubaydi, R.B. Figueiredo, Y. Huang, T.G. Langdon, *J. Mater. Sci.* **48**, 4661 (2013)
4. Y.J. Chen, Q.D. Wang, H.J. Roven, M. Karlsen, Y.D. Yu, M.P. Liu, J. Hjelen, *J. Alloy. Compd.* **462**, 192 (2008)
5. N. Pardis, B. Talebanpour, R. Ebrahimi, S. Zomorodian, *Mater. Sci. Eng. A* **528**, 7537 (2011)
6. S. Ahmadi, G. Faraji, V. Alimirzaloo, A. Donyavi, *Met. Mater. Int.* **27**, 2957 (2021)
7. A. Fattah-alhosseini, A.R. Ansari, Y. Mazaheri, M. Karimi, M. Haghshenas, *Mater. Sci. Eng. A* **688**, 218 (2017)
8. M. Mesbah, A. Fattahi, A.R. Bushroa, G. Faraji, K.Y. Wong, W.J. Basirun, A. Fallahpour, B. Nasiri-Tabrizi, *Met. Mater. Int.* **27**, 277 (2021)
9. G. Faraji, P. Yavari, S. Aghdamifar, M.M. Mashhadi, *J. Mater. Sci. Technol.* **30**, 134 (2014)
10. M. Mesbah, G. Faraji, A.R. Bushroa, *Met. Mater. Int.* **22**, 288 (2016)
11. M. Eftekhari, A. Fata, G. Faraji, M.M. Mashhadi, *J. Alloy. Compd.* **742**, 442 (2018)
12. A. Fata, M. Eftekhari, G. Faraji, M.M. Mashhadi, *J. Mater. Eng. Perform.* **27**, 2330 (2018)
13. H. Abdolvand, G. Faraji, M.K. Besharati Givi, R. Hashemi, M. Riazat, *Met. Mater. Int.* **21**, 1068 (2015)
14. M. Mesbah, F. Fadaeifard, A. Karimzadeh, B. Nasiri-Tabrizi, A. Rafieerad, G. Faraji, A.R. Bushroa, *Met. Mater. Int.* **22**, 1098 (2016)
15. A. Babaei, M.M. Mashhadi, *Prog. Nat. Sci.* **24**, 623 (2014)
16. A. Babaei, M.M. Mashhadi, H. Jafarzadeh, *J. Mater. Sci.* **49**, 3158 (2014)
17. M. Arzaghi, J.J. Fundenberger, L.S. Toth, R. Arruffat, L. Faure, B. Beausir, X. Sauvage, *Acta Mater.* **60**, 4393 (2012)
18. M.S. Mohebbi, A. Akbarzadeh, *Mater. Sci. Eng. A* **528**, 180 (2010)
19. B. Manafi, V. Shatermashhadi, K. Abrinia, G. Faraji, M. Sanei, *Int. J. Adv. Manuf. Tech.* **82**, 1823 (2016)
20. J. Skiba, W. Pachla, A. Mazur, S. Przybysz, M. Kulczyk, M. Przybysz, M. Wróblewska, *J. Mater. Process. Tech.* **214**, 67 (2014)
21. S.S. Jamali, G. Faraji, K. Abrinia, *Int. J. Adv. Manuf. Tech.* **88**, 291 (2017)
22. F. Samadpour, G. Faraji, P. Babaie, S.R. Bewsher, M. Mohammadpour, *Mater. Sci. Eng. A* **718**, 412 (2018)
23. A. Siah Sarani, F. Samadpour, M.H. Mortazavi, G. Faraji, *Met. Mater. Int.* **27**, 2933 (2021)
24. A. Siah Sarani, G. Faraji, *Arch. Civ. Mech. Eng.* **20**, 108 (2020)
25. G.I. Raab, E.P. Soshnikova, R.Z. Valiev, *Mater. Sci. Eng. A* **387-389**, 674 (2004)
26. S. Amani, G. Faraji, *Met. Mater. Int.* **25**, 1341 (2019)
27. M. Howeyze, A.R. Eivani, H. Arabi, H.R. Jafarian, N. Park, *J. Mater. Res. Technol.* **9**, 6682 (2020)
28. M. Howeyze, A.R. Eivani, H. Arabi, H.R. Jafarian, *Mater. Sci. Eng. A* **732**, 120 (2018)
29. K.K. Yogesha, A. Joshi, N. Kumar, R. Jayaganthan, *Mater. Manuf. Process.* **32**, 1336 (2017)
30. M. Moradpour, F. Khodabakhshi, H. Eskandari, *J. Mater. Res. Technol.* **8**, 630 (2019)
31. Loorentz, Y.G. Ko, *J. Alloy. Compd.* **586**, S205 (2014)
32. Y. Li, L. Li, J. Nie, Y. Cao, Y. Zhao, Y. Zhu, *J. Mater. Res.* **32**, 4443 (2017)
33. H. Jafarzadeh, K. Abrinia, *Mater. Charact.* **102**, 1 (2015)
34. R. Vafaei, M.R. Toroghinejad, R. Pippan, *Mater. Sci. Eng. A* **536**, 73 (2012)
35. N. Kamikawa, T. Furuhashi, *J. Mater. Process. Tech.* **213**, 1412 (2013)
36. C.P. Chang, P.L. Sun, P.W. Kao, *Acta Mater.* **48**, 3377 (2000)
37. V. Poojitha, T. Raghu, V. Pandurangadua, *Mater. Today Proc.* **18**, 2335 (2019)
38. P. Vishnu, R. Raj Mohan, E. Krishna Sangeetha, S. Raghuraman, R. Venkatraman, *Mater. Today Proc.* **21**, 212 (2020)
39. H. Lanjewar, S. Naghdy, P. Verleysen, L.A.I. Kestens, *Mater. Charact.* **160**, 110088 (2020)
40. S. Bagherzadeh, K. Abrinia, Q. Han, *J. Manuf. Process.* **50**, 485 (2020)
41. H. Lanjewar, S. Naghdy, F. Vercruyssen, L.A.I. Kestens, P. Verleysen, *Mater. Sci. Eng. A* **764**, 138195 (2019)
42. A. Mishra, V. Richard, F. Grégori, R.J. Asaro, M.A. Meyers, *Mater. Sci. Eng. A* **410-411**, 290 (2005)
43. N. Pardis, C. Chen, M. Shahbaz, R. Ebrahimi, L.S. Toth, *Mater. Sci. Eng. A* **613**, 357 (2014)
44. M. Mesbah, G. Faraji, A.R. Bushroa, *Mater. Sci. Eng. A* **590**, 289 (2014)

45. M.R. Toroghinejad, R. Jamaati, J. Dutkiewicz, J.A. Szpunar, *Mater. Design* **51**, 274 (2013)
46. T.G. Langdon, *Mater. Sci. Eng. A* **462**, 3 (2007)
47. S.S. Satheesh Kumar, T. Raghu, *Mater. Design* **57**, 114 (2014)
48. M. Alizadeh, E. Salahinejad, *Mater. Sci. Eng. A* **595**, 131 (2014)
49. S. Naghdy, L. Kestens, S. Hertelé, P. Verleysen, *Mater. Charact.* **120**, 285 (2016)
50. B. Omranpour, Y. Ivanisenko, R. Kulagin, L. Kommel, E.G. Sanchez, D. Nugmanov, T. Scherer, A. Heczal, J. Gubicza, *Mater. Sci. Eng. A* **762**, 138074 (2019)
51. R.Z. Valiev, T.G. Langdon, *Prog. Mater. Sci.* **51**, 881 (2006)
52. A.R. Eivani, F. Rahimi, *Mater. Sci. Eng. A* **745**, 159 (2019)
53. E.A. El-Danaf, *Mater. Sci. Eng. A* **487**, 189 (2008)
54. M. Reihanian, R. Ebrahimi, N. Tsuji, M.M. Moshksar, *Mater. Sci. Eng. A* **473**, 189 (2008)
55. Y. Ito, Z. Horita, *Mater. Sci. Eng. A* **503**, 32 (2009)
56. H. Torabzadeh Kashi, M. Bahrami, J. Shahbazi Karami, Gh. Faraji, *Iran. J. Mater. Sci. Eng.* **14**, 32 (2017)
57. J.F. Derakhshan, M.H. Parsa, H.R. Jafarian, *Mater. Sci. Eng. A* **747**, 120 (2019)
58. G.R. Ebrahimi, A. Barghamadi, H.R. Ezatpour, A. Amiri, *J. Manuf. Process.* **47**, 427 (2019)
59. R.Z. Valiev, *Mater. Sci. Eng. A* **234**, 59 (1997)
60. M. Moradpour, F. Khodabakhshi, S.R. Mohebpour, H. Eskandari, M. Haghshenas, *J. Manuf. Process.* **37**, 348 (2019)
61. M. Howeyze, H. Arabi, A.R. Eivani, H.R. Jafarian, *Mater. Sci. Eng. A* **720**, 160 (2018)
62. B. Wang, X.-H. Chen, F.-S. Pan, J.-J. Mao, Y. Fang, *T. Nonferr. Metal. Soc.* **25**, 2481 (2015)
63. H.R. Song, Y.S. Kim, W.J. Nam, *Met. Mater. Int.* **12**, 7 (2006)
64. T.L. Tsai, P.L. Sun, P.W. Kao, C.P. Chang, *Mater. Sci. Eng. A* **342**, 144 (2003)
65. G. Faraji, H.S. Kim, *Mater. Sci. Technol.* **33**, 905 (2017)
66. K. Bhansali, A.J. Keche, C.L. Gogte, S. Chopra, *Mater. Today Proc.* **26**, 3173 (2020)
67. X. Chen, G.-S. Huang, S.-S. Liu, T.-Z. Han, B. Jiang, A.-T. Tang, Y.-T. Zhu, F.-S. Pan, *T. Nonferr. Metal. Soc.* **29**, 437 (2019)
68. Y.M. Wang, E. Ma, *Acta Mater.* **52**, 1699 (2004)
69. H. Alvandi, K. Farmanesh, *Proc. Mater. Sci.* **11**, 17 (2015)
70. D.R. Fang, Q.Q. Duan, N.Q. Zhao, J.J. Li, S.D. Wu, Z.F. Zhang, *Mater. Sci. Eng. A* **459**, 137 (2007)
71. J. Deng, Y.C. Lin, S.-S. Li, J. Chen, Y. Ding, *Mater. Design* **49**, 209 (2013)
72. J. Jiang, T. Yuan, W. Zhang, A. Ma, D. Song, Y. Wu, *Mater. Sci. Eng. A* **733**, 385 (2018)
73. M. Ensafi, G. Faraji, H. Abdolvand, *Mater. Lett.* **197**, 121 (2017)

**Publisher's note** Springer Nature remains neutral with regard to jurisdictional claims in published maps and institutional affiliations.